Ultrasensitive Broadband Probing of Molecular Vibrational Modes with Multifrequency Optical Antennas

Heykel Aouani,[*,†] Hana Šípová,[‡] Mohsen Rahmani,[¶,§] Miguel Navarro-Cia,[∥,⊥] Kateřina Hegnerová,[‡] Jiří Homola,[‡] Minghui Hong,[§] and Stefan A. Maier[†]

[†]The Blackett Laboratory, Department of Physics, Imperial College London, London SW7 2AZ, United Kingdom, [‡]Institute of Photonics and Electronics, Academy of Sciences of the Czech Republic, Chaberska 57, 18251 Prague, Czech Republic, [¶]Data Storage Institute, (A*STAR) Agency for Science, Technology and Research, 5 Engineering Drive 1, Singapore 117608, [§]Department of Electrical and Computer Engineering, National University of Singapore, Singapore 117576, [∥]Department of Electronic & Electrical Engineering, University College London, London WC1E 7JE, United Kingdom, and [⊥]Optical and Semiconductor Devices Group, Department of Electrical and Electronic Engineering, Imperial College London, London SW7 2BT, United Kingdom

ABSTRACT Optical antennas represent an enabling technology for enhancing the detection of molecular vibrational signatures at low concentrations and probing the chemical composition of a sample in order to identify target molecules. However, efficiently detecting different vibrational modes to determine the presence (or the absence) of a molecular species requires a multispectral interrogation in a window of several micrometers, as many molecules present informative fingerprint spectra in the mid-infrared between 2.5 and 10 μm. As most nanoantennas exhibit a narrow-band response because of their dipolar nature, they are not suitable for such applications. Here, we propose the use of multifrequency optical antennas designed for operating with a bandwidth of several octaves. We demonstrate that surface-enhanced infrared absorption gains in the order of 10^5 can be easily obtained in a spectral window of 3 μm with attomolar concentrations of molecules, providing new opportunities for ultrasensitive broadband detection of molecular species *via* vibrational spectroscopy techniques.

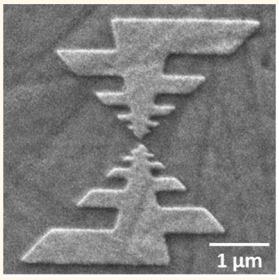

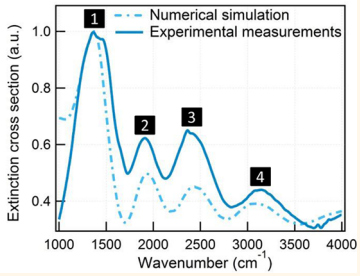

KEYWORDS: plasmonic · nanoantenna · broadband optical antenna · field enhancement · vibrational spectroscopy · SEIRA

Vibrational spectroscopy of molecules provides a unique chemical fingerprint of a material, making it an analytical tool of choice for life sciences, medicine, and biotechnologies. The probing of molecular vibrational modes is mainly performed *via* Raman or infrared absorption spectroscopy, and brings access to the chemical composition of a sample without prior knowledge. While Raman spectroscopy relies on an inelastic scattering occurring after light excitation at a higher frequency, infrared absorption spectroscopy is based on a direct excitation of the vibrational modes, leading to similar, but complementary, information for inversion-symmetric molecules.[1] Multispectral interrogation of vibrational signatures represents an accurate way for determining the molecular composition of a sample in order to confirm the presence (respectively the absence) of target molecular species, and reduces the number of false positives during biosensing experiments. However, because of the low cross section of these infrared processes (10−15 orders of magnitude smaller than typical fluorescence cross sections of dye molecules), efficiently detecting the multiple vibrational signatures of a sample at trace, or ultimately, single molecule level remains a challenging task. Therefore, improving the sensitivity of vibrational spectroscopy methods requires to invoke enhancement mechanisms such as resonant field enhancement on a broad range of frequencies.

Metallic nanodevices based on surface plasmon polaritons provide new routes to enhance light matter interactions in subwavelength volumes,[2] with major applications in molecular sensing,[3] light-emitting devices[4] and photovoltaics.[5] In this context, special attention was recently devoted to optical antennas, counterparts of radio and microwave antennas in the optical regime.[6−8]

* Address correspondence to h.aouani@imperial.ac.uk.

Received for review October 19, 2012 and accepted December 1, 2012.

Published online December 02, 2012
10.1021/nn304860t

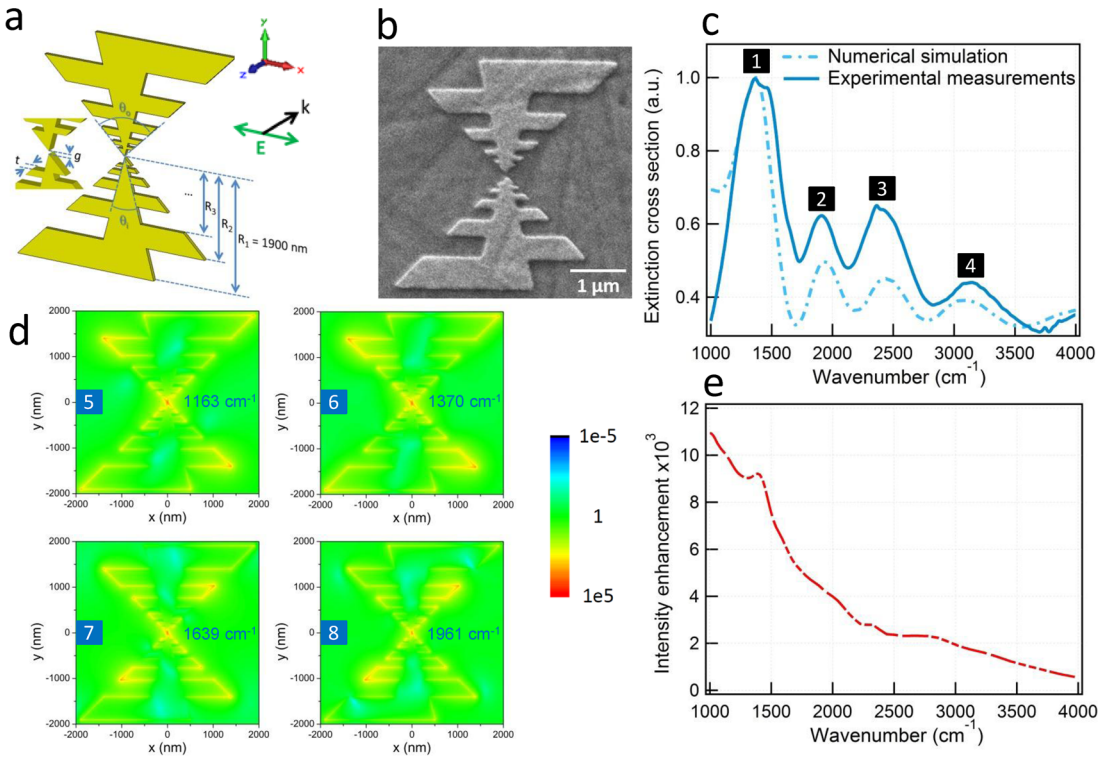

Figure 1. (a) Schematic geometry of the multifrequency gold optical antenna. (b) SEM image of a fabricated optical antenna, with geometrical parameters identical to the schematic in a. (c) Simulated (dash−dot line) and experimental (solid line) extinction cross sections of the optical antenna. The four resonance peaks are numbered from the fundamental (1) to the fourth resonance (4). (d) Intensity enhancement of the electric field with respect to the incident field ($|E(x,y)|^2/|E_0|^2$) 2 nm above the surface for wavenumbers at 1163 cm^{-1} (5), 1370 cm^{-1} (6), 1639 cm^{-1} (7), and 1961 cm^{-1} (8) when the optical antenna is illuminated by an *x*-polarized plane-wave. (e) Intensity enhancement of the electric field with respect to the incident field ($|E(0,0,0)|^2/|E_0|^2$) at the center of the optical antenna when illuminated by an *x*-polarized plane-wave.

By reversibly converting propagating electromagnetic waves into localized energy and modifying the emission properties of individual quantum emitters,[9−13] optical antennas appear to be essential devices to enhance fluorescence spectroscopy of molecules fixed on a substrate[14] or diffusing in solution,[15,16] Raman spectroscopy,[17−21] and infrared absorption spectroscopy.[22−25] However, such optical antennas exhibit a narrow-band response and hence are not suitable for multispectral sensing of biomolecules. Proposing efficient nanodevices operating in a large spectral window is a current challenge to be addressed for multispectral biosensing on the same substrate.

Optical antennas operating in a broad range of frequencies have been recently proposed to enhance nonlinear light matter interactions during second[26,27] and third order nonlinear processes,[28,29] thus introducing the concept of multifrequency optical antennas. By designing the nanoantenna with a bandwidth of several octaves, a high intensity enhancement of the electric fields can be obtained in a spectral window of several micrometers. However, up to this point, the broadband properties of such devices have not been yet exploited for biochemical sensing applications.

In this paper, we report the realization of broadband log-periodic trapezoidal nanoantennas ideally designed for multispectral surface-enhanced infrared absorption (SEIRA) spectroscopy. An experimental demonstration of multispectral ultrasensitive infrared sensing was performed using alkanethiol molecules adsorbed on individual gold optical antennas, leading to SEIRA gains greater than 10^5 in a spectral window of 3 μm. This opens promising opportunities for the development of biosensors suitable for multispectral sensing on the same chip.

RESULTS AND DISCUSSION

To facilitate the design and final assessment of the performance of the experimental log-periodic trapezoidal optical antenna array, finite-difference time-domain (FDTD) simulations (Lumerical FDTD Solutions v7.5) were performed for a single optical antenna. Figure 1 shows the design together with relevant FDTD simulation results. The geometry of the gold (Au) trapezoidal nanoantenna is defined by the following parameters: $R_{m+1}/R_m = (0.54)^{1/2}$ with $m = 1,2,...,9$, $R_1 = 1900$ nm; inner and outer angles $\theta_i = 30°$ and $\theta_o = 90°$, respectively; metal thickness t = 45 nm; and gap between arms g = 20 nm (Figure 1a). These dimensions match those inferred from the high-resolution scanning electron microscopy (SEM) images of the fabricated samples (Figure 1b), but neglect fabrication asymmetries and

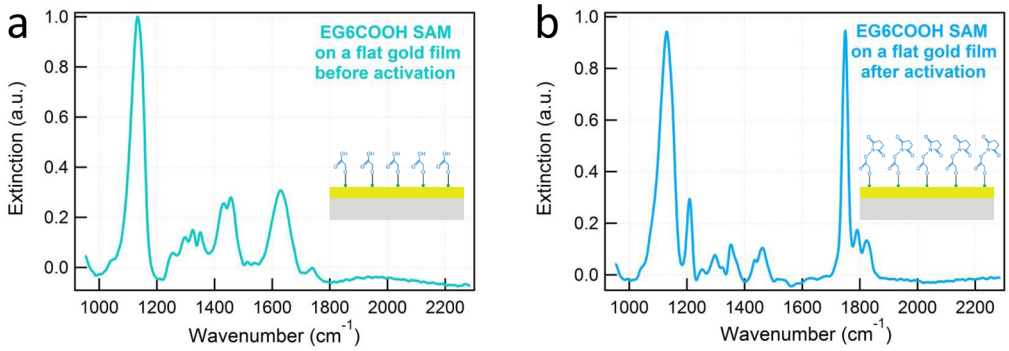

Figure 2. Infrared extinction spectrum of alkanethiol molecule before (a) and after (b) treatment of EDC and NHS mixture measured in the case of adsorption on a flat gold film under grazing illumination.

imperfections. In addition, the nanoantenna rests over a 3 nm thick titanium (Ti) adhesion layer and a semi-infinite barium fluoride (BaF_2) substrate. The multifrequency nanoantenna was illuminated from the semi-infinite air space with a *x*-polarized plane-wave propagating along -*z*. As can be see in Figure 1c, the extinction cross section of the nanoantenna displays a fundamental resonance peak at 1370 cm^{-1} (7300 nm), and three resonance peaks respectively centered at 1923 cm^{-1} (5200 nm), 2439 cm^{-1} (4100 nm), and 3125 cm^{-1} (3200 nm), which overlap with each other preventing the extinction cross section from decreasing to zero. Each resonance is related to a pair of induced horizontal dipoles, which, in turn, induces a local vertical dipole between arms, as previously reported in ref 29 (see Supporting Information for more details). The electromagnetic field enhancement (defined as $|E(x,y)|^2/|E_0|^2$, where $|E_0|^2$ is the amplitude of the incident field) provided by the multifrequency nanoantenna 2 nm above the surface is displayed in Figure 1d for several wavenumbers corresponding to our area of interest. This distance is considered as representative for the sensing mechanism since the binding monolayer used has an estimated thickness of 2 nm. Lastly, the field enhancement at the gap only ($|E(0,0,0)|^2/|E_0|^2$, the origin of the coordinate axis is considered to be at the very center of the gap defined by the two arms of the nanoantenna) is plotted in Figure 1e for wavenumbers ranging from 1150 to 4000 cm^{-1}. A high electromagnetic enhancement is expected with this multifrequency optical antenna in a bandwidth of several octaves, ideally designed for multispectral infrared sensing (see details in Methods).

The trapezoidal optical antennas were fabricated by using electron-beam lithography and standard lift-off process (see Methods for more details about the fabrication process), with geometrical parameters identical to those described in Figure 1a. The surface morphology of the optical antenna was characterized by high-resolution scanning electron microscopy (SEM) and atomic force microscopy (AFM). A representative SEM image of an individual nanoantenna is presented in Figure 1b, and a 3D AFM image is available in the Supporting Information.

The extinction spectrum of the fabricated structures (defined as 1-transmission) was measured by Fourier transform infrared spectroscopy (FTIR, Bruker Hyperion 2000) through a square array of approximately 150 nanoantennas (pitch of 10 μm) at normal incidence under linear polarization. This 10 μm pitch ensured that coupling between neighboring nanoantennas was insignificant, as confirmed by numerical simulations. We point out that the number of nanoantennas used in our experiments can be drastically reduced by using a synchrotron light, as this excitation light source allows single nanoantenna measurements with a good signal-to-noise ratio. The measured extinction spectrum of the trapezoidal gold nanoantenna array has been superimposed on the simulated spectrum of Figure 1c, where the detected fundamental resonance of the nanoantenna is centered at 1410 cm^{-1} (7092 nm), and the resonances at larger wavenumbers are respectively measured at 1910 cm^{-1} (5236 nm), 2400 cm^{-1} (4167 nm), and 3150 cm^{-1} (3175 nm), which agrees very well with the numerical simulations.

The broadband SEIRA activity of our trapezoidal optical antenna was investigated by functionalizing the structures with self-assembled monolayers (SAM) of carboxyl-terminated alkanethiols AT-EG_6-COOH (HS-C_{11}-EG_6-OCH_2—COOH from Prochimia, Poland). To probe the infrared absorption enhancement in a broad spectral window, the vibrational signatures of the SAM have been measured before and after treatment with a mixture of 1-ethyl-3-(3-dimethylaminopropyl)-carbodiimide (EDC) and *N*-hydroxysuccinimide (NHS), corresponding to the conversion of the carboxylic group of AT-EG_6-COOH to NHS ester. The reference infrared spectra of AT-EG_6-COOH before and after activation with EDC and NHS have been determined in the case of adsorption on a flat gold film under grazing illumination and are respectively presented in Figure 2a,b. Please note that this data will be used hereafter as a reference to compute the SEIRA gains brought by the broadband nanoantennas. The molecular SAM before and after activation exhibits several infrared active vibrational signatures from 1000 to 1800 cm^{-1}. We point out that our research work is motivated by

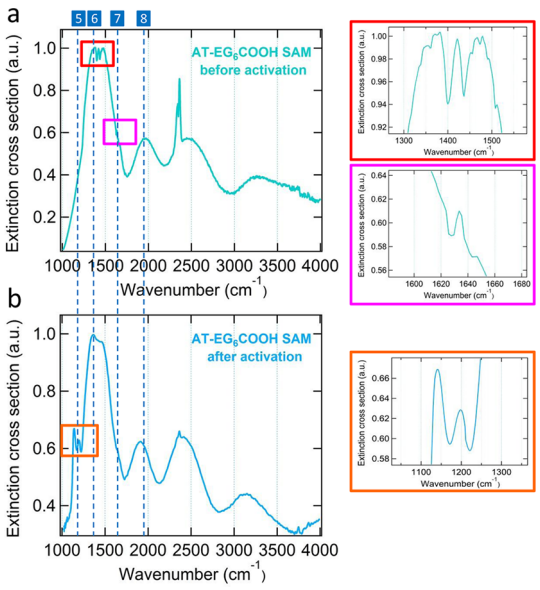

Figure 3. Experimental extinction cross section of the multifrequency optical antenna adsorbed with alkanethiol molecules before (a) and after (b) treatment of EDC and NHS mixture. Peaks around 2362 cm^{-1} are due to CO_2 absorption. Vertical dashed lines indicate the wavenumbers of the intensity maps presented in Figure 1d.

high security and defense needs, as enhancing infrared absorption signals in a spectral window of several micrometers would improve the sensitivity detection of target molecular species at trace level such as trinitrotoluene (TNT), and reduce the number of false positives *via* a multispectral interrogation of the vibrational modes. As AT-EG$_6$-COOH presents strong vibrational signatures in the mid-infrared part of the electromagnetic spectrum and in particular from 1000 to 1800 cm^{-1}, these molecules are used in this paper as TNT mimetic molecules. The results that we will present below can be extended to experimental configurations corresponding to TNT molecules adsorbed on metallic film.

The interactions between the alkanethiol molecules, before treatment with EDC and NHS, and the multifrequency nanoantennas are presented in Figure 3a. The extinction spectrum of the nanoantennas presents a similar overall shape as the initial infrared spectrum measured (Figure 1c), but the fundamental resonance profile is affected by the appearance of strong dips around 1400, 1434, and 1627 cm^{-1}, which is characteristic of a Fano antiresonance profile.[22] Since these dips in the extinction spectrum of the nanoantennas are not observed before adsorption of the SAM (Figure 1c), we conclude that these Fano signatures are originated from the coupling between the nanoantennas and the vibrational modes of the AT-EG$_6$-COOH molecules in this region. This Fano profile results from the quantum antiphase interactions between the enhanced electromagnetic field associated to the broad resonance of the trapezoidal nanoantenna, and the narrow field resonance corresponding to the vibrational active

TABLE 1. SEIRA Factors for the Different Vibrational Modes Analyzed Computed Using Figure 3a,b

wavenumber (cm^{-1})	SEIRA factor
1139	0.8×10^5
1200	1.4×10^5
1400	1.9×10^5
1434	1.9×10^5
1627	0.8×10^5

modes of AT-EG$_6$-COOH molecules in this spectral window[30−32] (υ_{CH2} scissoring vibration at 1400 cm^{-1}, υ_{CH2} asymmetrical deformation vibration at 1434 cm^{-1} and $\upsilon_{asym,sym,COO-}$ in deprotonated form of −COOH at 1627 cm^{-1}), as previously reported.[22] The detected vibrational signal size, defined as the difference between the maximum and minimum extinction at the vibrational mode feature, respectively reaches values of 6.2% at 1400 cm^{-1}, 5.3% at 1434 cm^{-1}, and 2% at 1627 cm^{-1}.

The previous extinction profile differs after conversion of the AT-EG$_6$-COOH acid group into NHS ester. As we can see in Figure 3b, two neighboring Fano dips appear in the infrared spectrum at 1171 and 1221 cm^{-1}, respectively, corresponding to the vibrational modes of the crystalline structure and amorphous layer in AT-EG$_6$ (υ_{COC}).[33,34] Such high interactions between the activated AT-EG$_6$-COOH SAM and the multifrequency optical antennas are made possible due to the strong electromagnetic field enhancement generated out of the fundamental resonance peak (Figure 1d). From this set of data, the signal size is estimated to 7.3% at 1171 cm^{-1} and 3.8% at 1221 cm^{-1}.

We are now able to determine the infrared absorption enhancement provided by the trapezoidal optical antennas. To this end, we define the SEIRA factor as the ratio between the average signal amplitude per molecule with the optical antenna for the vibrational mode studied as compared to the average signal amplitude per molecule in the case of adsorption on the flat gold film. The average signal amplitude per molecule has been determined by normalizing the overall molecular infrared signal amplitude from a single optical antenna for the target vibrational mode, by the number of AT-EG$_6$-COOH molecules adsorbed. The concentration of AT-EG$_6$-COOH molecules has been deduced knowing the bulk occupied by a molecule in the SAM and the dimension of the adsorbed optical antenna. Results are presented in Table 1. Experimental SEIRA gains greater than 0.9×10^5 were obtained for the different vibrational modes, with a maximum enhancement at 1400 and 1434 cm^{-1}, where the estimated gains reach values up to 1.9×10^5. This infrared amplification of the vibrational signal comes from the contributions of electromagnetic and chemical enhancement mechanisms, as previously highlighted.[35−38] However, determining the respective weight of each contribution participating to

the overall SEIRA gain is a difficult task, and is out of the scope of this paper. The electromagnetic enhancement mechanism can be nevertheless qualitatively correlated with the intensity enhancement 2 nm above the nanoantenna (which corresponds to the SAM thickness) presented in Figure 1d.

The broadband properties of the trapezoidal nanoantennas provide infrared absorption enhancement of the adsorbed molecules in the order of 10^5 in a spectral window of 3 μm. As each nanoantenna is covered by alkanethiol molecules at attomolar concentrations (less than 1.2×10^6 molecules), the proposed broadband nanodevice represents a powerful tool for multispectral enhanced-detection of molecular vibrational signatures with high sensitivity. The analysis spectral window associated to the extinction cross section of the multifrequency optical antennas could be expanded by optimizing several parameters of the design, thus increasing the electromagnetic intensity enhancement provided by the nanoantennas in the spectral region corresponding to secondary resonances. This can be accomplished by reducing the gap between the two elements, optimizing the adhesion layer between the gold film and the glass substrate,[39] or tuning the geometrical parameters of the metallic teeth,[29] but nevertheless requires overcoming the nanofabrication challenges.

CONCLUSIONS

We have reported in this paper a multispectral enhanced detection of the vibrational signatures from alkanethiol molecules adsorbed on trapezoidal optical antennas. By designing the optical antenna with a bandwidth of several octaves, a broadband electromagnetic intensity enhancement is generated in its vicinity. SEIRA enhancement factors in the order of 10^5 were experimentally provided for alkanethiol molecules at attomolar concentrations, in a spectral window of 3 μm. The next step of our research work is to functionalize the samples with molecules localized at the gap only, in order to exploit the full broadband properties of the trapezoidal nanoantenna at the hot spot. Experimental measurements would be conducted with TNT molecules, in order to efficiently detect plastic explosives at trace level, and reduce the number of false positives by probing several vibrational modes. We believe that these results could open new opportunities for biosensing including ultrasensitive multispectral vibrational detection and simultaneous identification of different molecular species.

METHODS

Numerical Simulations. Extinction cross section and near-field field distributions is calculated using the 3D finite-difference time-domain (FDTD) commercial software Lumerical FDTD Solutions v7.5. The optical dielectric functions of gold (Au) and titanium (Ti) taken from Palik,[40] are fitted by a built-in, multi-coefficient model in the FDTD software: five and six coefficients were used for Au and Ti, respectively. The BaF_2 is assumed to be dispersionless with an index of refraction $n = 1.465$.[41] Perfect matched layers are defined as boundary conditions of our simulation volume at a distance with respect to the nanoantenna of at least one wavelength. To reduce computational effort, the total-field scattered-field (TFSF) source is used. A nonuniform mesh with overridden subgridding volumes is used to discretize the simulation volume such that the different length scales involved in the solution of the Maxwell's equations are treated accurately and the fine details of the geometry are modeled precisely. The default cubic grid of the region defined by the TFSF source is set to 12 nm $\times$ 12 nm $\times$ 10 nm. The mesh is further increased to 7 nm $\times$7 nm $\times$ 5 nm in the rectangular cuboid enclosing the six smallest teeth of the nanoantenna. A mesh size 1 nm $\times$ 1 nm $\times$ 1 nm and 2 nm $\times$ 2 nm $\times$ 0.5 nm are overridden over the volume enclosing the gap between the arms and the adhesion layer, respectively. The maximum simulation time is set as 300 fs. The time stepping stability factor is set to 0.95, which corresponds to a time step of $t = 0.00129$ fs. The residual energy in the calculation volume is 1×10^5 of its peak value to ensure that the simulation has run for a sufficiently long time for the CW information obtained by Fourier transformations to be valid. The convergence of the simulations against the residual energy in the simulation volume, the mesh, and the performance of the perfect matched layers at the boundaries is checked following the same procedure as in ref 29.

The nanoantenna is illuminated with a *x*-polarized plane-wave propagating along -*z*, and thus, incident from semi-infinite free-space. The extinction cross-section σ_{ext} is calculated with the solver defined script by the sum of the power flowing outward through a rectangular cuboid enclosing the TFSF source and the net power flowing inward through a rectangular cuboid enclosing the nanoantenna, but not the TFSF source. A probe monitor and a 2D field profile monitor recorded the electromagnetic field strengths at the center of the nanoantenna and at the *xy*-cross-sectional plane 2 nm above the Au-air interface, respectively.

Fabrication of Trapezoidal Nanoantennas. The structural geometries are fabricated by electron-beam lithography (Elonix 100KV EBL system) in poly(methyl methacrylate) (PMMA) positive resist, accompanied with standard lift-off process. The substrate used for this research work is BaF_2 with a thickness of 1 mm. To avoid charging, a 20 nm Espacer is coated on the resist. The sample possesses a footprint of 150 μm $\times$ 150 μm in which arrays of antennas with a pitch of 10 μm are fabricated. Structures consist of 3 nm Ti adhesion layer and 40 nm Au thin film, which are deposited by e-beam evaporation (EB03 BOC Edwards).

FTIR Measurements. The infrared absorption measurements have been conducted using a commercial FTIR setup (Bruker Hyperion 2000). For measurements in the mid-infrared regime, we used a MCT detector cooled with liquid nitrogen (hold time approximately 8 h). During normal operation, purging the microscope interior is not necessarily required. However, purging the optics with dry air or nitrogen gas (dew point < -40 °C, that corresponds to 128 ppm humidity) reduces the peak intensity of water vapor, CO_2, or other environmental contaminants in the middle infrared region of the spectrum. During the purging operation, the maximum pressure should not exceed 2 bar and the gas low rate 300 L/hour. The purge gas pressure can be regulated by installing a pressure control valve between the purge gas line and the purge gas inlet. The experimental extinction spectra have been obtained by integrating the infrared signal from an optical antenna array (4 nm resolution, 1000 scans). The absorption of the BaF_2 substrate has been taken into account by subtracting it to the previous spectrum, before being normalized by the excitation source profile (determined by using a silver mirror), thus giving access to the extinction spectrum displayed in Figure 1c.

Functionalization of the Samples. A self-assembled monolayer (SAM) of carboxy-terminated alkanethiols is used as a model biomolecular system for infrared absorption spectroscopy. Details of the functionalization procedure are given below. The substrate is thoroughly rinsed with ethanol and cleaned in UV-ozone cleaner for 5 min. Carboxyl-terminated alkanethiols $HS\text{-}C_{11}\text{-}EG_6\text{-}OCH_2\text{—}COOH$ (Prochimia, Poland) are dissolved in ethanol (purity ≥99.9%, Merck, USA) at a concentration of 200 μM. The clean substrate is immersed in the solution of the thiols at 40 °C for 10 min and stored at room temperature overnight. Then the substrate is rinsed with ethanol, dried with stream of nitrogen, and stored under argon atmosphere. To activate the carboxylic groups, the sample is incubated for 10 min in an aqueous solution of 0.5 M 1-ethyl-3-(3-dimethylaminopropyl)-carbodiimide (EDC) and 0.1 M *N*-hydroxysuccinimide (NHS) (from GE Healthcare, USA). Then, the substrate is rinsed with deionized water and dried with a stream of nitrogen.

Conflict of Interest: The authors declare no competing financial interest.

Acknowledgment. We thank Victor Torres for his help on the modeling work, Tyler Roschuk for his help during the preparation of the samples, and Binni Varghese for AFM images. H.A. acknowledges stimulating discussions with Yan Francescato. This work was supported by the U.S. Army International Technology Centre Atlantic (USAITC-A) and the Office of Naval Research (ONR and ONR Global). M.N.-C. is supported by the Imperial College Junior Research Fellowship.

Supporting Information Available: Additional numerical simulations of the multifrequency optical antennas and raw experimental data. This material is available free of charge *via* the Internet at http://pubs.acs.org.

REFERENCES AND NOTES

1. Larkin, P. J. *IR and Raman Spectroscopy*; Jones and Bartlett Publishers, Inc: Burlington, MA, 2005.
2. Maier, S. A. *Plasmonics: Fundamentals and Applications*; Springer: New York, 2007.
3. Fu, Y.; Lakowicz, J. R. Modification of Single Molecule Fluorescence near Metallic Nanostructures. *Laser Photonics Rev.* **2009**, *3*, 221–232.
4. Schuller, J. A.; Barnard, E. S.; Cai, W. S.; Jun, Y. C.; White, J. S.; Brongersma, M. L. Plasmonics for Extreme Light Concentration and Manipulation. *Nat. Mater.* **2010**, *9*, 193–204.
5. Atwater, H. A.; Polman, A. Plasmonics for Improved Photovoltaic Devices. *Nat. Mater.* **2010**, *9*, 205–213.
6. Bharadwaj, P.; Deutsch, B.; Novotny, L. Optical Antennas. *Adv. Opt. Photonics* **2009**, *1*, 438–483.
7. Novotny, L.; van-Hulst, N. F. Antennas for Light. *Nat. Photonics.* **2011**, *5*, 83–90.
8. Giannini, V.; Fernández-Domínguez, A. I.; Sonnefraud, Y.; Roschuk, T.; Fernández-García, R.; Maier, S. A. Controlling Light Localization and Light—Matter Interactions with Nanoplasmonics. *Small* **2010**, *6*, 2498–2507.
9. Anger, P.; Bharadwaj, P.; Novotny, L. Enhancement and Quenching of Single-Molecule Fluorescence. *Phys. Rev. Lett.* **2006**, *96*, 113002.
10. Kühn, S.; Håkanson, U.; Rogobete, L.; Sandoghdar, V. Enhancement of Single-Molecule Fluorescence using a Gold Nanoparticle as an Optical Nanoantenna. *Phys. Rev. Lett.* **2006**, *97*, 017402.
11. Muskens, O. L.; Giannini, V.; Sanchez-Gil, J. A.; Gomez Rivas, J. Strong Enhancement of the Radiative Decay Rate of Emitters by Single Plasmonic Nanoantennas. *Nano Lett.* **2007**, *7*, 2871–2875.
12. Curto, A.; Volpe, G.; Taminiau, T. H.; Kreuzer, M.; Quidant, R.; Van Hulst, N. F. Unidirectional Emission of a Quantum Dot Coupled to a Nanoantenna. *Science* **2010**, *329*, 930–933.
13. Aouani, H.; Itzhakov, S.; Gachet, D.; Devaux, E.; Ebbesen, T. W.; Rigneault, H.; Oron, D.; Wenger, J. Colloidal Quantum Dots as Probes of Excitation Field Enhancement in Photonic Antennas. *ACS Nano* **2010**, *4*, 4571–4578.
14. Kinkhabwala, A.; Yu, Z. F.; Fan, S. H.; Avlasevich, Y.; Mullen, K.; Moerner, W. E. Large Single-Molecule Fluorescence Enhancements Produced by a Bowtie Nanoantenna. *Nat. Photonics* **2009**, *3*, 654–657.
15. Aouani, H.; Mahboub, O.; Bonod, N.; Devaux, E.; Popov, E.; Rigneault, H.; Ebbesen, T. W.; Wenger, J. Bright Unidirectional Fluorescence Emission of Molecules in a Nanoaperture with Plasmonic Corrugations. *Nano Lett.* **2011**, *11*, 637–644.
16. Aouani, H.; Mahboub, O.; Devaux, E.; Rigneault, H.; Ebbesen, T. W.; Wenger, J. Plasmonic Antennas for Directional Sorting of Fluorescence Emission. *Nano Lett.* **2011**, *11*, 2400–2406.
17. Yan, B.; Thubagere, A.; Premasiri, W. R.; Ziegler, L. D.; Dal Negro, L.; Reinhard, B. M. Engineered SERS Substrates with Multiscale Signal Enhancement: Nanoparticle Cluster Arrays. *ACS Nano* **2009**, *3*, 1190–1202.
18. Brolo, A. G.; Arctander, E.; Gordon, R.; Leathem, B.; Kavanagh, K. L. Nanohole-Enhanced Raman Scattering. *Nano Lett.* **2004**, *4*, 2015–2018.
19. Ward, D. R.; Grady, N. K.; Levin, C. S.; Halas, N. J.; Wu, Y.; Nordlander, P.; Natelson, D. Electromigrated Nanoscale Gaps for Surface-Enhanced Raman Spectroscopy. *Nano Lett.* **2007**, *7*, 1396–1400.
20. Jackson, J. B.; Halas, N. J. Surface-Enhanced Raman Scattering on Tunable Plasmonic Nanoparticle Substrates. *Proc. Natl. Acad. of Sci. U.S.A.* **2004**, *101*, 17930–17935.
21. Zhang, W.; Fischer, H.; Schmid, T.; Zenobi, R.; Martin, O. J. F. Mode-Selective Surface-Enhanced Raman Spectroscopy Using Nanofabricated Plasmonic Dipole Antennas. *J. Phys. Chem. C* **2009**, *113*, 14672–14675.
22. Neubrech, F.; Pucci, A.; Cornelius, T. W.; Karim, S.; Garcia-Etxarri, A.; Aizpurua, J. Resonant Plasmonic and Vibrational Coupling in a Tailored Nanoantenna for Infrared Detection. *Phys. Rev. Lett.* **2008**, *101*, 157403.
23. Pryce, I. M.; Aydin, K.; Kelaita, Y. A.; Briggs, R. M.; Atwater, H. A. Highly Strained Compliant Optical Metamaterials with Large Frequency Tunability. *Nano Lett.* **2010**, *10*, 4222–4227.
24. Giannini, V.; Francescato, Y.; Amrania, H.; Phillips, C. C.; Maier, S. A. Fano Resonances in Nanoscale Plasmonic Systems: A Parameter-Free Modeling Approach. *Nano Lett.* **2011**, *11*, 2835–2840.
25. Rahmani, M.; Luk'yanchuk, B.; Hong, M. Fano Resonance in Novel Plasmonic Nanostructures. *Laser Photonics Rev.* **2012**, 10.1002/lpor.201200021.
26. Aouani, H.; Navarro-Cia, M.; Rahmani, M.; Sidiropoulos, T. P H; Hong, M.; Oulton, R. F; Maier, S. A. Multiresonant Broadband Optical Antennas as Efficient Tunable Nanosources of Second Harmonic Light. *Nano Lett.* **2012**, *12*, 4997–5002.
27. Thyagarajan, K.; Rivier, S.; Lovera, A.; Martin, O. J. F. Enhanced Second-Harmonic Generation from Double Resonant Plasmonic Antennae. *Opt. Express* **2012**, *20*, 12860–12865.
28. Harutyunyan, H.; Volpe, G.; Quidant, R.; Novotny, L. Enhancing the Nonlinear Optical Response Using Multifrequency Gold-Nanowire Antennas. *Phys. Rev. Lett.* **2012**, *108*, 217403.
29. Navarro-Cia, M.; Maier, S. A. Broad-Band Near-Infrared Plasmonic Nanoantennas for Higher Harmonic Generation. *ACS Nano* **2012**, *6*, 3537–3544.
30. Zorn, S.; Dettinger, U.; Skoda, M. W. A.; Jacobs, R. M. J.; Peisert, H.; Gerlach, A.; Chassé, T.; Schreiber, F. Stability of Hexa(ethylene glycol) SAMs Towards the Exposure to Natural Light and Repeated Reimmersion. *Appl. Surf. Sci.* **2012**, *258*, 7882–7888.
31. Briand, E.; Salmain, M.; Compère, C.; Pradier, C.-M. Immobilization of Protein A on SAMs for the Elaboration of Immunosensors. *Colloids Surf., B* **2006**, *53*, 215–224.
32. Briand, E.; Salmain, M.; Herry, J.-M.; Perrot, H.; Compère, C.; Pradier, C.-M. Building of an Immunosensor: How Can the Composition and Structure of the Thiol Attachment Layer Affect the Immunosensor Efficiency? *Biosens. Bioelectron.* **2006**, *22*, 440–448.
33. Briand, E.; Humblot, V.; Pradier, C.-M.; Kasemo, B.; Svedhem, S. An OEGylated Thiol Monolayer for the Tethering of Liposomes and the Study of Liposome Interactions. *Talanta* **2010**, *81*, 1153–1161.

34. Cao, C.; Sim, S. J. Signal Enhancement of Surface Plasmon Resonance Immunoassay Using Enzyme Precipitation-Functionalized Gold Nanoparticles: A Femto Molar Level Measurement of Anti-glutamic Acid Decarboxylase Antibody. *Biosens. Bioelectron.* **2007**, *22*, 1874–1880.
35. Osawa, M.; Ikeda, M. Surface-Enhanced Infrared Absorption of *p*-Nitrobenzoic Acid Deposited on Silver Island Films: Contribution of Electromagnetic and Chemical Mechanisms. *J. Phys. Chem.* **1991**, *95*, 9914–9919.
36. Merklin, G. T.; Griffith, P. R. Influence of Chemical Interactions on the Surface-Enhanced Infrared Absorption Spectrometry of Nitrophenols on Copper and Silver Films. *Langmuir* **1997**, *13*, 6159–6163.
37. Krauth, O.; Fahsold, G.; Pucci, A. Asymmetric Line Shapes and Surface Enhanced Infrared Absorption of CO Adsorbed on Thin Fe Films on MgO(001). *J. Chem. Phys.* **1999**, *110*, 3113–3117.
38. Alonso-González, P.; Albella, P.; Schnell, M.; Chen, J.; Huth, F.; Garca-Etxarri, A.; Casanova, F.; Golmar, F.; Arzubiaga, L.; Hueso, L. E.; *et al.* Resolving the Electromagnetic Mechanism of Surface-Enhanced Light Scattering at Single Hot Spots. *Nat. Commun.* **2012**, *3*, 684.
39. Aouani, H.; Wenger, J.; Gérard, D.; Rigneault, H.; Devaux, E.; Ebbesen, T. W.; Mahdavi, F.; Xu, T.; Blair, S. Crucial Role of the Adhesion Layer on the Plasmonic Fluorescence Enhancement. *ACS Nano* **2009**, *3*, 2043–2048.
40. Palik, E. D. *Handbook of Optical Constants of Solids*; Academic Press: San Diego, CA, 1998.
41. Crystran Ltd. http://www.crystran.co.uk.